PLOS ONE

RESEARCH ARTICLE

# Cutaneous transcriptome analysis in NIH hairless mice

**Zhong-Hao Ji☯, Jian Chen☯, Wei Gao, Jin-Yu Zhang, Fu-Shi Quan, Jin-Ping Hu, Bao Yuan*, Wen-Zhi Ren***

Department of Laboratory Animals, College of Animal Sciences, Jilin University, Changchun, Jilin, China

☯ These authors contributed equally to this work.
* rwz1964@163.com (WZR); yuan_bao@jlu.edu.cn (BY)





**Citation:** Ji Z-H, Chen J, Gao W, Zhang J-Y, Quan F-S, Hu J-P, et al. (2017) Cutaneous transcriptome analysis in NIH hairless mice. PLoS ONE 12(8): e0182463. https://doi.org/10.1371/journal.pone.0182463

**Editor:** Andrzej T Slominski, University of Alabama at Birmingham, UNITED STATES

**Received:** March 22, 2017

**Accepted:** July 19, 2017

**Published:** August 7, 2017



**Data Availability Statement:** All relevant data are within the paper and its Supporting Information files.

**Funding:** This study was supported by the National Key Technology R&D Program (2015BAI07B02), National Natural Science Foundation of China (31501954), and Natural Science Foundation of Jilin Province (20170623034TC). The funders had no role in study design, data collection and analysis, decision to publish, or preparation of the manuscript.

## Abstract

Mice with spontaneous coat mutations are ideal animal models for studying skin development and tumorigenesis. In this study, skin hair growth cycle abnormalities were examined in NIH hairless mice 42 days after birth (P42) by using hematoxylin-eosin (H&E) staining. To examine the gene expression patterns in the skin of mutant mice, the dorsal skin of P42 female NIH mice and NIH hairless mice was sequenced by RNA-Seq, and 5,068 differentially expressed genes (DEGs) were identified (false discovery rate [FDR] $\geq 2$, $P < 0.05$). A pathway analysis showed that basal cell carcinoma, the cell cycle and the Hippo, Hedgehog and Wnt signaling pathways were up-regulated in NIH hairless mice. Previous studies have shown that these pathways are closely associated with cell proliferation, cell cycle, organ size and cancer development. In contrast, signal transduction, bacterial and parasitic infection, and receptor-mediated pathways, including calcium signaling, were down-regulated in NIH hairless mice. A gene interaction network analysis was performed to identify genes related to hair follicle development. To verify the reliability of the RNA-Seq results, we used q-PCR to analyze 12 key genes identified from the gene interaction network analysis, including eight down-regulated and four up-regulated genes, and the results confirmed the reliability of the RNA-Seq results. Finally, we constructed the differential gene expression profiles of mutant mice by RNA-Seq. NIH hairless mice exhibited abnormalities in hair development and immune-related pathways. *Pik3r1* and *Pik3r3* were identified as key genes, laying the foundation for additional in-depth studies of hairless mice.

## Introduction

Hair follicle growth and development have a certain periodicity and include three stages: anagen, catagen and telogen. The control of these processes is important in hair generation and degradation [1, 2]. Mice with spontaneous coat mutations are useful animal models for the study of hair follicle development and hair growth [3–5], and studies of skin follicle growth and development have received increasing attention [6, 7]. Currently, researchers are focusing on the growth phenotype and changes in hair growth caused by certain mutations as well as the biological principles and molecular mechanisms underlying these characteristics [8, 9]. The use of mice with spontaneous coat mutations and targeted genetic engineering will

**Competing interests:** The authors have declared that no competing interests exist.

provide invaluable information for the study of the mechanisms and principles of hair development disorders [10].

In our previous study, selected biological characteristics of NIH hairless mouse were studied, thereby providing a research basis for the study of this mouse model with a mutation affecting the coat and hair.[11]. To understand the hair development state, we observed the skin structure at the time points embryonic stage 16.5(E16.5), postnatal day 3(P3), P7, P12, P16, P21, P28, P33, P37, P42, and P60 by H&E staining (although only the results of P7 and P42 are shown), and we found significant differences between the phenotypes and pathology of the skin of the mice at P42. Through inbreeding, we established a mutant mouse strain with hair follicle development and growth cycle disorders (NIH hairless mice), making this strain a good animal model for studying human diseases.

Transcriptome sequencing is used to study transcripts of particular tissues or organs of a species in a particular state and is superior to microarrays in terms of information volume and accuracy [12]. By constructing a transcriptome library, we can obtain information about transcripts and alternative splicing and can determine the differential expression patterns of specific genes [13–16].

In the present study, the expression patterns of skin-related genes in NIH hairless mice at P42 were examined by RNA-Seq, and these patterns were then compared with those in NIH normal mice. Through Gene Ontology (GO), pathway and differentially expressed gene (DEG) interaction network analyses, the potential associations between these DEGs and hair follicle development were analyzed to identify key genes important in the development of the mouse hair follicle. The differences in some DEGs were then validated by q-PCR.

## Materials and methods

### Ethics statement

All animal experiments were approved by the Institutional Animal Care and Use Committee (IACUC) of Jilin University. The animal experiments were performed in accordance with the requirements of the Experimental Animal Ethics and Welfare guidelines (Permit Number: 20160205).

### Histological analysis of NIH normal and NIH hairless mice

SPF-grade female NIH hairless and NIH normal mice of the strain SCXK-2011-0003 (201600 017738) were originally purchased from the Institute of Biological Products Co., Ltd(Changchun, China). Mice were bred in the Laboratory Animal Center of Jilin University. In the place of the back midline's right and one centimeter above the tail, scissor a lump of skin whose length is around one centimeter and width is about 0.25 centimeter at postnatal day 7 (P7) and P42. Skin samples were embedded in paraffin, fixed, cut into 6-μm slices, and subjected to hematoxylin-eosin (H&E) staining following a standard method. Images were acquired on an optical microscope (Olympus, Tokyo, Japan).

### Sample preparation

Six-week-old female NIH hairless and NIH normal mice were sacrificed by cervical dislocation (n = 5 per group). In the place of the back midline's right and one centimeter above the tail, scissor a lump of skin whose length is around 0.5 centimeter and width is about 0.25 centimeter, and total RNA was extracted with TRIzol reagent following the manufacturer's instructions (Invitrogen, Carlsbad, CA, USA). The RNA quality was determined on a Bioanalyzer 2200 (Agilent), and the samples were stored at −80˚C. RNA with an RIN > 6.0 was used for cDNA library construction.

## GO analysis

GO analysis was applied to analyze the main functions of the DEGs according to Gene Ontology [17]. Fisher's exact tests and $\chi^2$ tests were used to classify the GO categories, and the false discovery rate (FDR) [18] was calculated to correct the P-value (smaller FDRs indicated a smaller error in judging the P-values). The FDR was defined as FDR = 1—$N_k$ / T, where $N_k$ refers to the number of Fisher's test P-values that were less than the $\chi^2$ test P-values. The P-values for the GO annotations of all DEGs were calculated. Enrichment provides a measure of the significance of the function: as the enrichment increases, the corresponding function is more specific, which helps us determine the GO categories with more concrete descriptions. Within the significant category, the enrichment Re was given by Re = ($n_f$ / n) / ($N_f$ / N), where $n_f$ is the number of DEGs within the particular category, n is the total number of genes within the same category, $N_f$ is the number of DEGs in the entire microarray, and N is the total number of genes in the microarray [19].

## Pathway analysis

A pathway analysis was performed to determine the significant DEG pathways. Pathway annotations were downloaded from the Kyoto Encyclopedia of Genes and Genomes (KEGG) database (http://www.genome.jp/Kegg/). Fisher's exact test was used to identify the enriched pathways. The resulting P-values were adjusted using the Benjamini-Hochberg (BH) FDR algorithm [20]. Pathway categories with an FDR $< 0.05$ were selected for further analysis.

Enrichment provides a measure of the significance of the function; as the enrichment increases, the corresponding function is more specific, which helps us determine the significant pathways. The enrichment was calculated as enrichment = ($n_g$ / n) / ($N_g$ / n), where $n_g$ is the number of DEGs within the particular pathway, $n_a$ is the total number of genes within the same pathway, $n_g$ is the number of DEGs with at least one pathway annotation, and $n_a$ is the number of genes with at least one pathway annotation in the entire microarray.

## Gene interaction network analysis

The KEGG database was used to build a network of genes based on the relationships between the genes, proteins and compounds in the database [21–24].

## Co-expression network

For a comprehensive analysis of the expressed genes that takes into account all significantly differentially expressed transcripts, we used a well-described (unsupervised) methodology for gene correlation network analysis to cluster transcripts into groups of highly interconnected modules based on a topological overlap mapping method known as weighted gene correlation network analysis (WGCNA) [25].

Within the network analysis, degree centrality is the simplest and most important measure of the centrality of a gene within a network, indicating its relative importance. Degree centrality is defined as the number of links that one node has with another [26]. Moreover, to examine the network properties, W-cores were introduced in order to simplify the graph topology analysis. A W-core is a subnetwork in which all nodes are connected to at least W other genes in the subnetwork. A W-core of a protein-protein interaction network usually contains cohesive groups of proteins [26, 27]. The purpose of the network structure analysis is to locate core regulatory factors (genes) in one network, with core regulatory factors defined as those that connect the most adjacent genes and have the highest degrees. The core regulatory factors were determined by the differences in degree between two class samples [28]. These factors always have the largest differences in degree.

## Real-time q-PCR analysis

Real-time q-PCR was performed to validate the gene expression data obtained from the RNA-Seq analysis. Total RNA was reverse-transcribed using TRIzol (Invitrogen, Carlsbad, CA, USA) according to the manufacturer's instructions. Approximately 1 μg of total RNA was used for first-strand cDNA synthesis. Each q-PCR contained 2 μL of DNA template, 12.5 μL of SYBR Fast q-PCR Mix (Takara, Tokyo, Japan), 8.5 μL of $ddH_2O$, 1 μL of upstream primer F and 1 μL of downstream primer R in a final volume of 25 μL. The q-PCR reaction parameters included a 15-s denaturation step at 95˚C and 40 cycles of 95˚C for 5 s and 60˚C for 30 s followed by a melting curve analysis. The primer pairs used for q-PCR amplification were designed using Integrated DNA Technologies (IDT, http://sg.idtdna.com/site). The CT value in the fluorescent quantitative reaction indirectly represents the expression level of the gene, and the relative quantification of gene expression can be achieved by comparison with a housekeeping gene. In this experiment, *Actb* was used as the internal reference, and relative gene expression was calculated using the following formula: ΔΔCt = ΔCt (case)—ΔCt (control), with the difference determined according to $2^{-\Delta\Delta Ct}$ [29].

## Immunohistochemistry

The proteins Pik3r1 and Pik3r3 in tissue sections from female NIH normal and NIH hairless mice at P7 and P42 were detected using the SABC method. Tissue sections (6 μm) from each group were dehydrated in xylene and a graded ethanol series, and other reagents were added in the following order: primary antibody [Pik3r1 (1:300), Pik3r3 (1:300); rabbit polyclonal

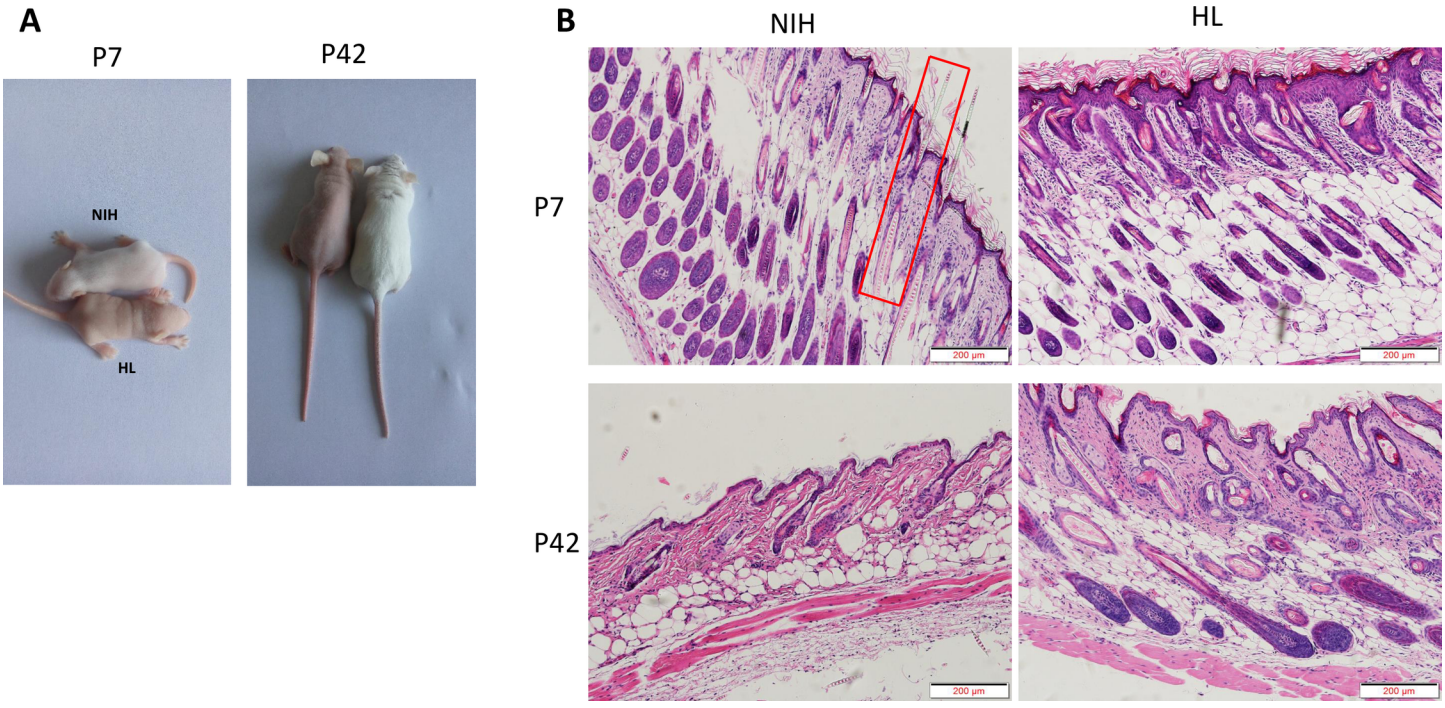


**Fig 1. Phenotypes of NIH hairless and NIH normal mice.** A: Hair loss in seven- and 42-day-old HL (NIH hairless) and NIH (NIH normal) mice. At P7, body hair completely covers NIH mice, whereas HL mice have completely bare pink skin. B: Histological features of HL mice at P7 and P42. H&E-stained sections show the arrangement of neat, normally growing hair follicles (HFs) and hair shafts in NIH mice at P7 (displayed in the red box). In HL mice, the hair shaft cannot penetrate the epidermis. At P42, the HFs of NIH normal mice exhibited normal cycling. In contrast, the subcutaneous fat layer of HL mice contains abnormal hair follicles and hair follicle development cycle abnormalities. Bar = 200 microns.

https://doi.org/10.1371/journal.pone.0182463.g001

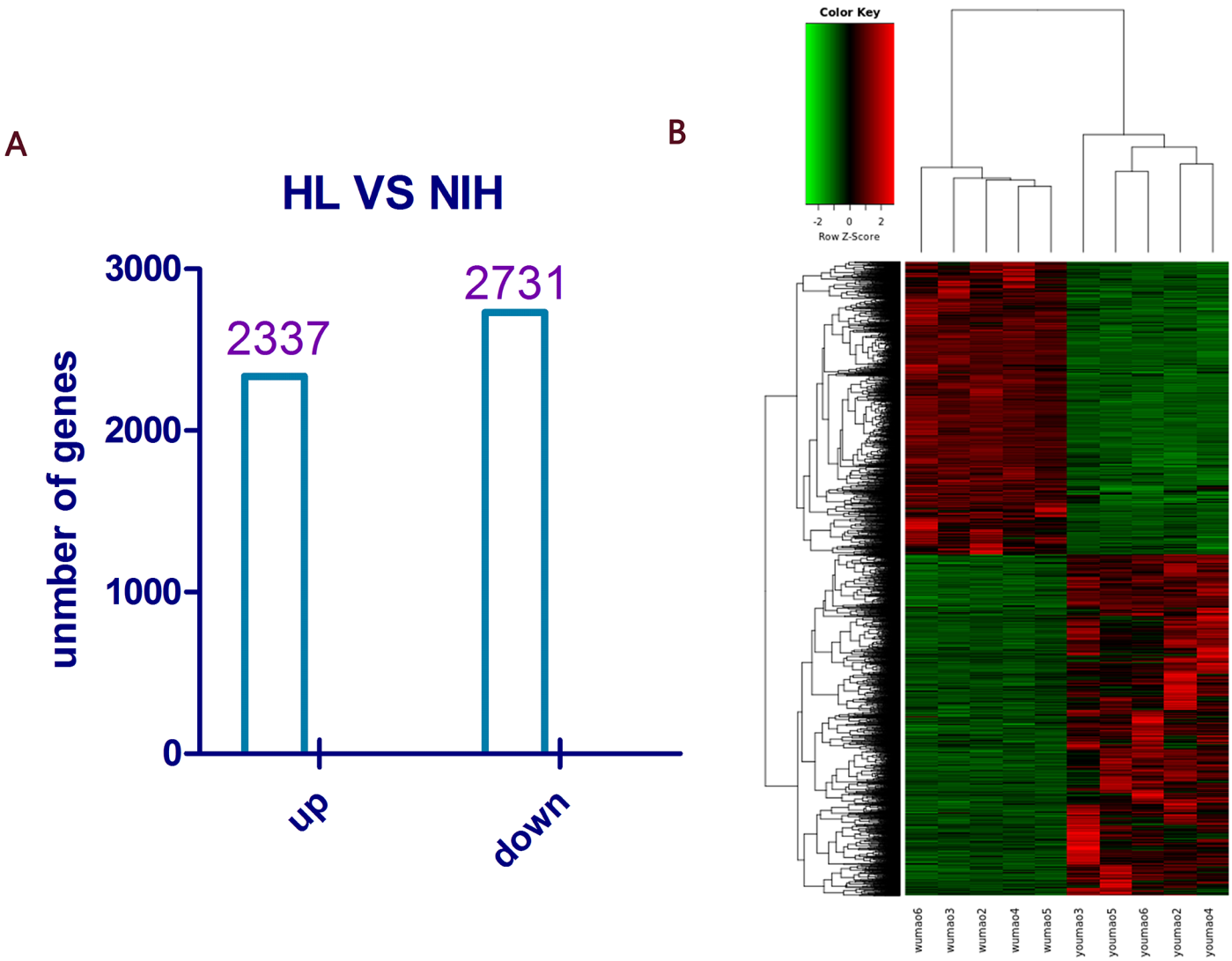


**Fig 2. Gene expression profiles in HL mouse skin using RNA-Seq.** A: In total, 5,068 DEGs (FDR ≥ 2, P < 0.05) were obtained after sequencing analysis, and these included 2,337 up-regulated genes and 2,731 down-regulated genes. B: Hierarchical clustering represents the differential expression of genes in the skin between NIH hairless and NIH normal mice. There were five repetitions within each group.

https://doi.org/10.1371/journal.pone.0182463.g002

antibodies, BBI, Shanghai, China)], biotinylated secondary antibody, SABC reagents and DAB solution (Wuhan Boster Co, Wuhan, China.). The sections were then rinsed in distilled water, dehydrated using alcohol and xylene, mounted on coverslips using permanent mounting medium and observed under an optical microscope equipped with a 10× objective (Olympus, Tokyo, Japan). For negative controls, the slides were treated with PBS instead of the primary antibody.

## Results

### Phenotypic descriptions

NIH normal and NIH hairless mice appeared identical at birth. At P7, NIH mice were completely covered with body hair, whereas the NIH hairless (HL) mice retained their bare pink skin (Fig 1A). With age, the HL mice grew sparse hair and had clearly distinct histological

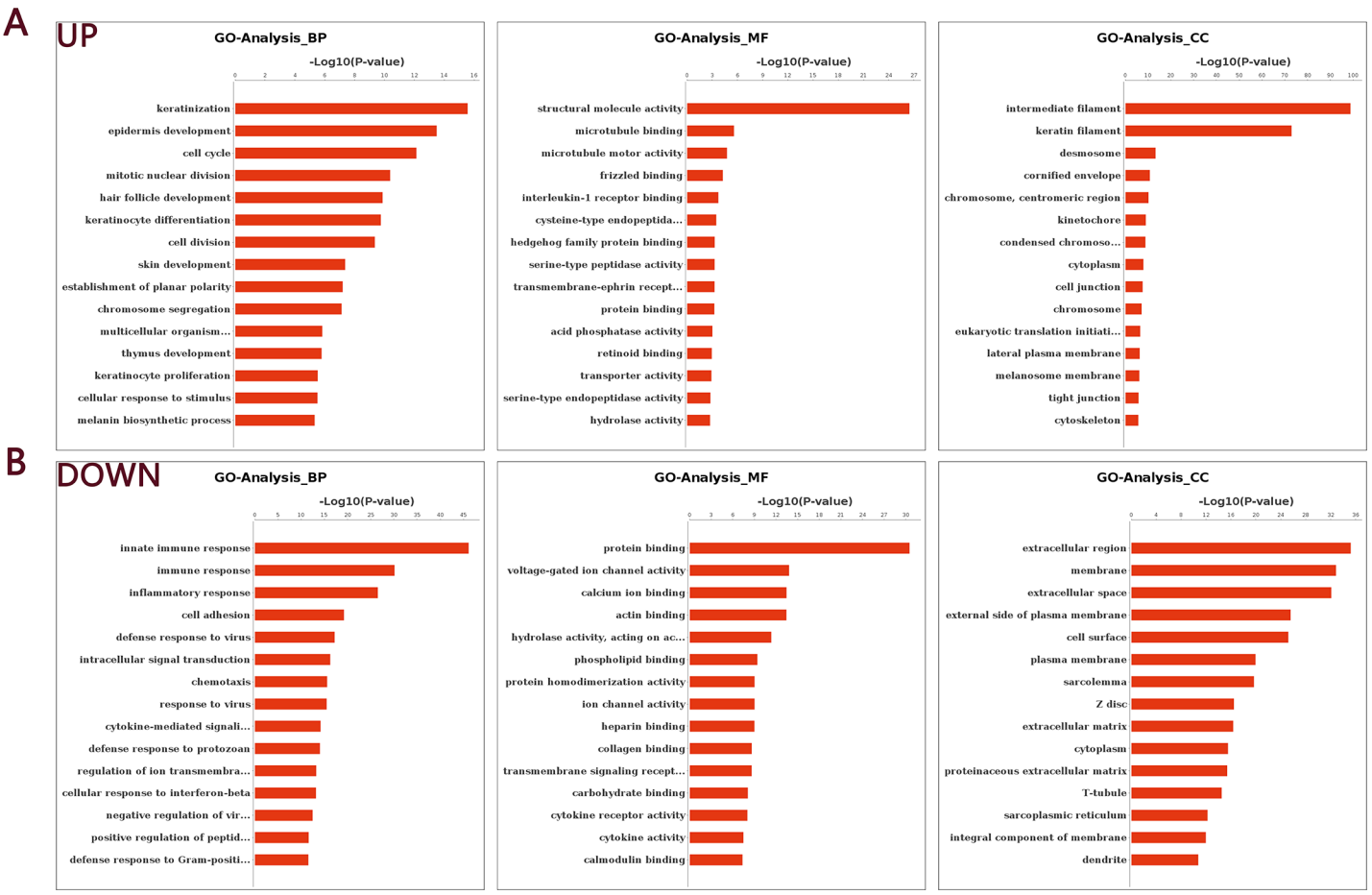


**Fig 3. GO analysis of all differentially expressed unigenes.** A: Up-regulated genes in the skin of NIH HL and NIH normal mice. B: Down-regulated genes in the skin of NIH HL and NIH normal mice.

https://doi.org/10.1371/journal.pone.0182463.g003

features at P7 and P42. The H&E-stained sections of the NIH mouse skin showed neatly arranged hair follicles (HFs) and normal growth at P7. At P42, the HFs of NIH normal mice exhibited normal cycling. Conversely, the subcutaneous tissue fat layer of HL mice contained abnormal hair follicles and showed abnormal hair follicle development (Fig 1B).

## RNA-Seq analysis of NIH normal and NIH hairless mice

RNA-Seq libraries were constructed from NIH normal and HL mice. Fast-QC (http://www.bioinformatics.babraham.ac.uk/projects/fastqc/) software was used to evaluate the quality of the sequencing data, which included the base quality value distribution, position distribution, GC content and PCR duplication content. The quality control results are shown in S1 Table. Map Splice software was used to compare the RNA-Seq data. The mapping statistics are shown in S1 Table.

## Identification of DEGs

We examined the expression of 22,426 genes. Differential gene expression analysis of the control (NIH normal mice) and case (NIH hairless mice) groups was performed using the DESeq algorithm.

We obtained a total of 5,068 DEGs, of which 2,337 were up-regulated and 2,731 were down-regulated (Fig 2; see S1 File for details).

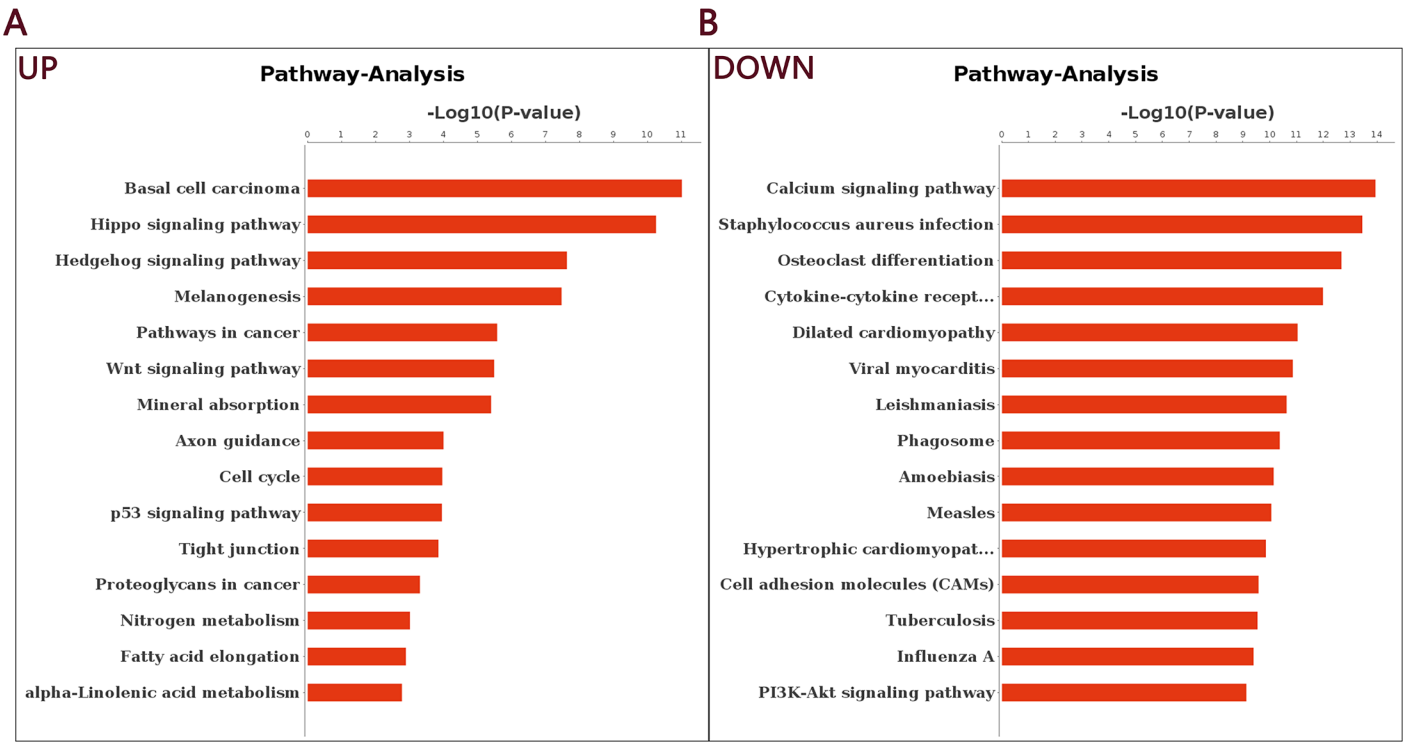


**Fig 4. Pathway analysis of all differentially expressed unigenes.** A: Up-regulated genes in the skin of NIH HL and NIH normal mice. B: Down-regulated genes in the skin of NIH HL and NIH normal mice.

https://doi.org/10.1371/journal.pone.0182463.g004

## GO and pathway analysis

GO enrichment analysis was performed on the RNA-Seq data. Among the 5,068 DEGs, 4,188 were annotated to 1,256 significant biological process GO categories ($P < 0.05$); 4,271 were annotated to 170 significant cell component GO categories ($P < 0.05$); and 4,152 were annotated to 334 significant molecular function GO categories ($P < 0.05$). As shown in Fig 3, keratinization, epidermis development, cell cycle, mitotic nuclear division, hair follicle development, keratinocyte differentiation and skin development were associated with genes that were highly expressed in NIH HL mice, whereas genes that were weakly expressed in NIH HL mice were mainly associated with the innate immune response, the immune response, the inflammatory response, cell adhesion and defense responses to virus infection (see S2–S4 Files for details).

We then used the KEGG database to analyze pathways associated with the DEGs and identified 37 up-regulated pathways and 118 down-regulated pathways. The comparison between NIH hairless and NIH normal mice showed that the DEGs were associated with immunity, cell cycle, apoptosis, cancer and microbial infection. Fig 4 presents the up- and down-regulated pathways obtained from pathway analysis and sorted by confidence level. The GO and pathway analyses allowed us to preliminarily classify the DEGs, which will provide important information for the screening of functional genes (see S5 File for details).

## Weighted gene co-expression network analysis

The WGCNA clustered 5,068 transcripts into four co-expression modules. The module conservation across all datasets is shown as a dendrogram in (Fig 5). Based on WGCNA convection, the four enriched modules were colored turquoise, yellow, brown and blue. Among

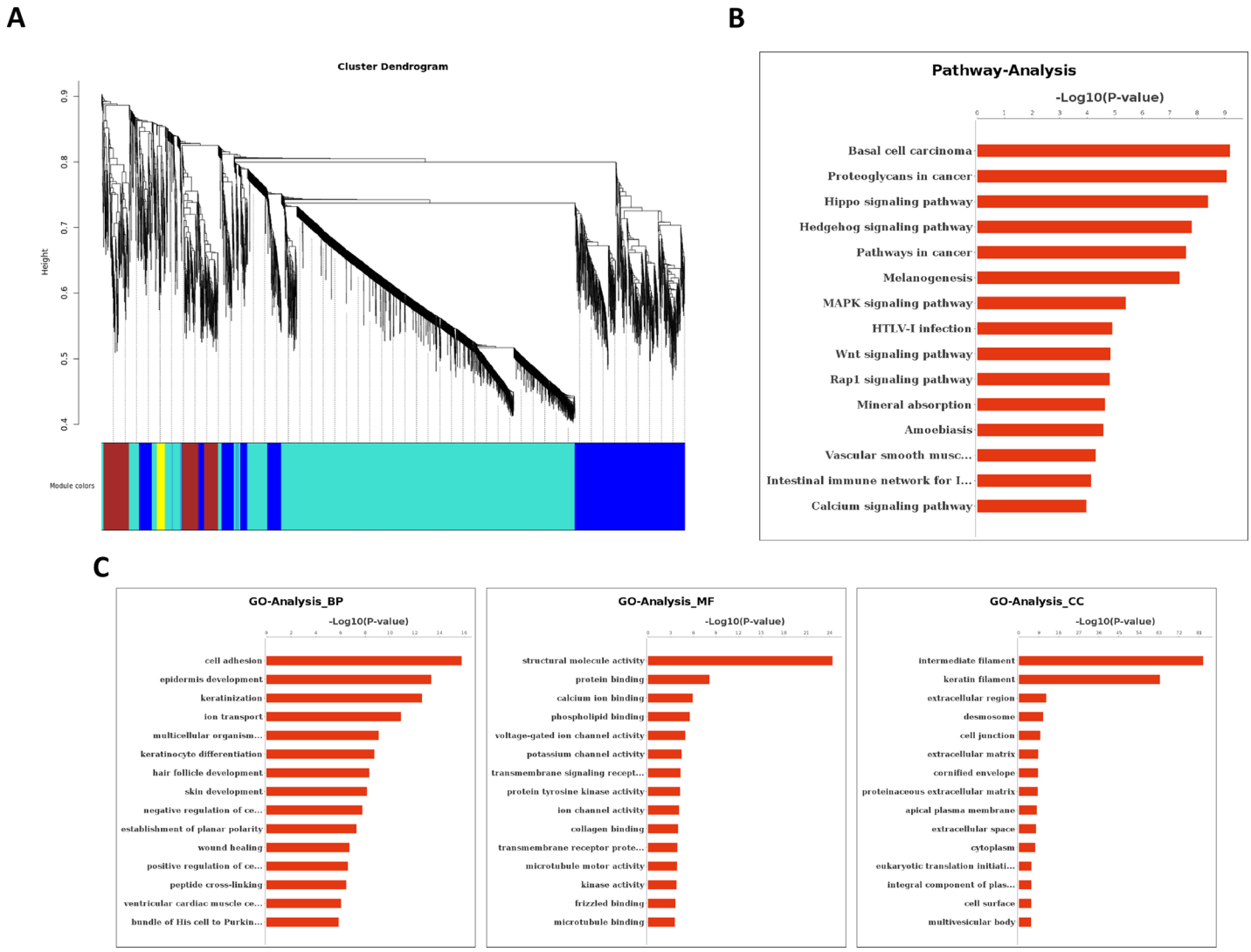


**Fig 5. Results of the weighted co-expression analysis of DEGs using the WGCNA algorithm.** A: Network heat map. The branch in the hierarchical cluster tree corresponds to the module. B: Relationships between HL and NIH module traits. Different colors represent different classification modules. C: GO analysis of DEGs in the turquoise module. D: Pathway analysis of DEGs in the turquoise module.

https://doi.org/10.1371/journal.pone.0182463.g005

them, the turquoise module (Fig 5) represents the genes of interest and shows the 838 DEGs identified and the results of the GO and pathway analyses (see S6 File for details).

## Gene interaction network and pathway interaction network analyses

To further study the interactions between genes and the internal links between pathways, we built two gene interaction networks and one pathway interaction network based on the KEGG database. We first chose genes that were not associated with human diseases to build the gene interaction network (Fig 6). In total, 628 DEGs were included in this network, in which red represents the down-regulated genes and green represents the up-regulated genes in the experimental group. The degree is arranged based on the degree of involvement of the genes in the network. Genes in the PI3K family, including *Pik3r1*, *Pik3r3* and *Pik3cd*, were identified as

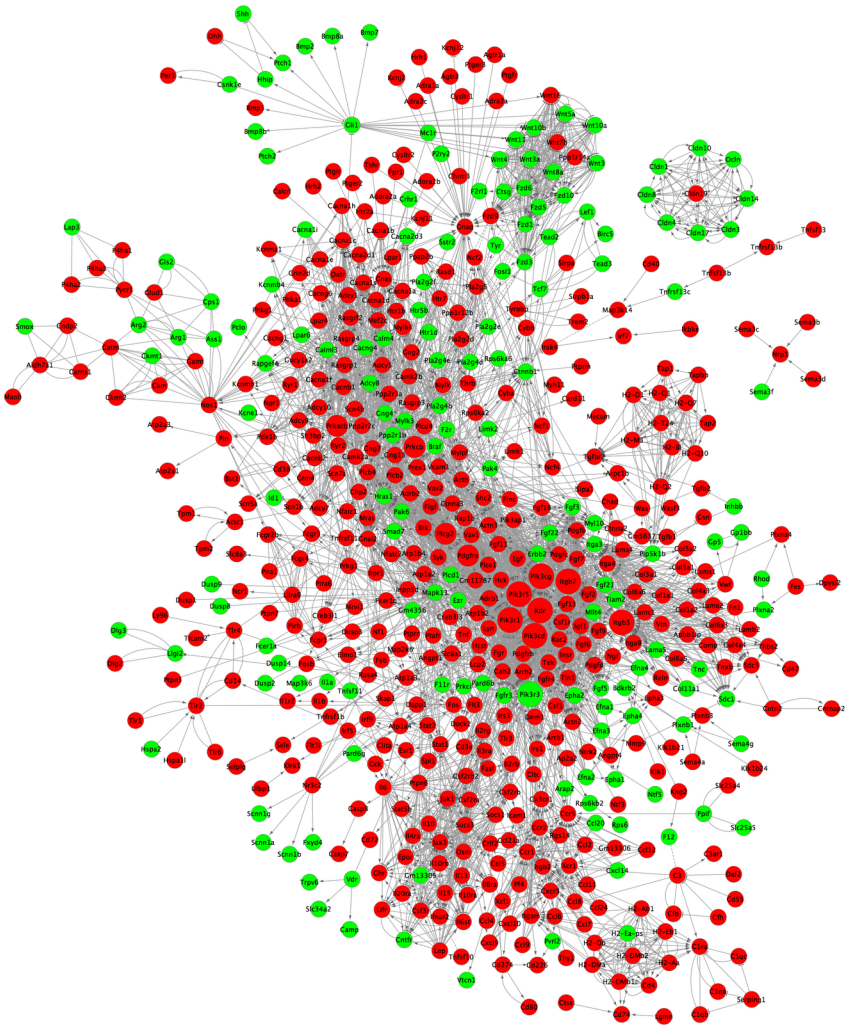

**Fig 6. Gene interaction network and pathway interaction network analyses.** For genes that are not associated with human diseases, larger dots correspond to higher degrees of participation in the interaction network. Red represents down-regulated genes, and green represents up-regulated genes.

https://doi.org/10.1371/journal.pone.0182463.g006

core genes. We also analyzed the differences in DEGs associated with human diseases. The gene interaction network (Fig 7A) showed that the PI3K family members were still situated at the core of the network. We also built a pathway interaction network between human diseases and organismal systems (Fig 7B).

## Confirmation of RNA-Seq results by q-PCR

To ensure that our sequencing data were true and reliable, we selected several relatively important genes obtained from the gene interaction network analysis, four up-regulated genes (*Krt17*, *Plxna2*, *Pik3r3* and *Ctse*) and eight down-regulated genes (*Pik3r1*, *Pik3cd*, *Itgb3*, *Kdr*, *Gnaq*, *Htra3*, *Jak1* and *Pik3r5*) (12 total), which were verified by q-PCR (Fig 8). The results obtained from the two methods were consistent for each gene (see S7 File for details).

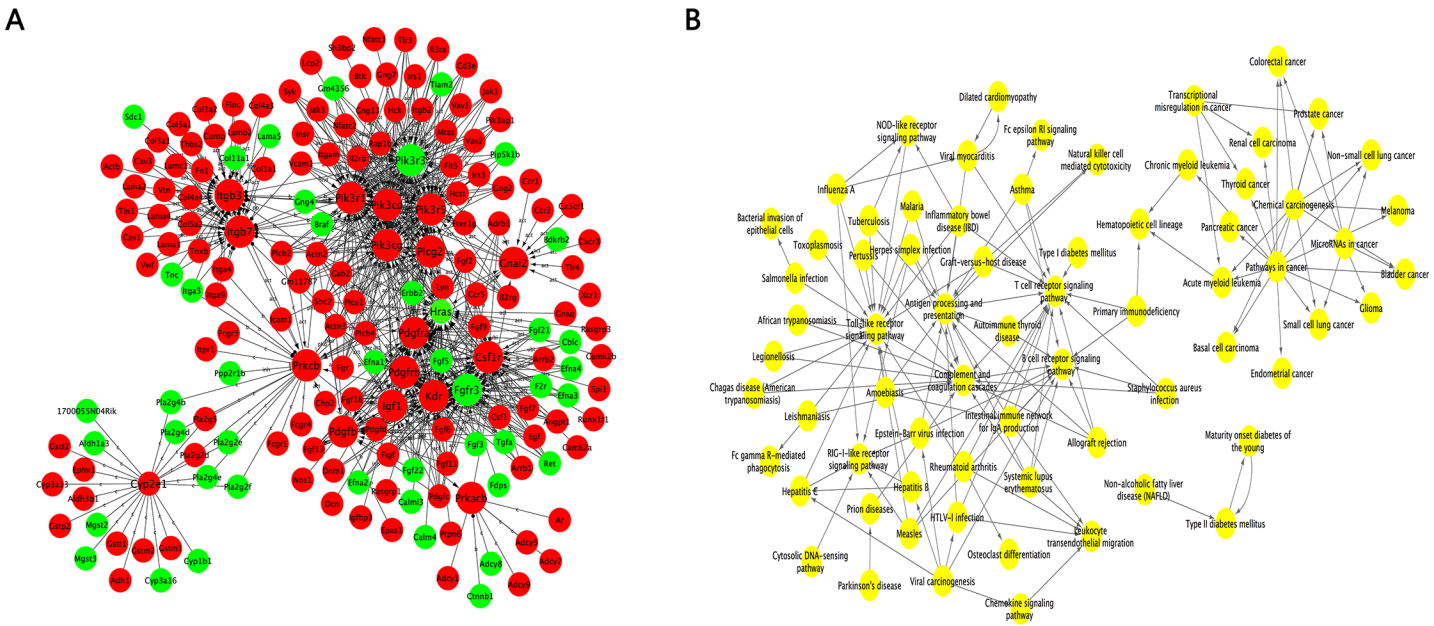


**Fig 7. Gene interaction network and pathway interaction network analyses.** A: For genes that are associated with human diseases and immune pathways, larger dots correspond to higher degrees of participation in the interaction network. Red represents down-regulated genes, and green represents up-regulated genes. B: The pathway interaction network between human diseases and organismal systems. Circular nodes represent pathways, and an arrow between two nodes represents an interaction target between pathways.

https://doi.org/10.1371/journal.pone.0182463.g007

## Expression of Pik3r1 and Pik3r3 proteins in tissue sections

To study the relationship between the *Pik3r1* and *Pik3r3* genes and hair development, we used immunohistochemistry to observe the expression of these two proteins in the skin. We found that the Pik3r1 and Pik3r3 proteins were mainly expressed in the hair follicles, even though the sebaceous glands also showed some levels of Pik3r1 and Pik3r3 expression. Interestingly, although these two proteins were both found in some hair follicles and were not expressed in others, we hypothesized that this result was related to whether the hair follicles were active or inactive. However, the specific evidence for this phenomenon requires further in-depth studies (Figs 9 and 10).

## Discussion

Mice with spontaneous coat mutations are useful animal models for the study of hair follicle development and hair growth [30]. The skin is the body's first immune barrier. The functions of the skin are integrated into the skin immune, pigmentary, epidermal and adnexal systems and are in continuous communication with the systemic immune, neural and endocrine systems [31]. Mice with skin mutations often exhibit immune dysfunctions, which indicates that bodily infections also have important implications for immunity [32]. Previous studies have shown that the skin is affected by the regulation of corticotropin-releasing factor (CRF), which produces some direct or indirect phenotypic effects that can regulate epidermal barrier function and the skin immune, pigmentary, adnexal, and dermal functions necessary to maintain local and systemic homeostasis [33, 34]. To date, several hairless mouse strains have been used to investigate immune responses, tumorigenesis, skin development and other research questions. Some such models are nude mice with *Foxn1* gene mutations; these mice lack thymic cell immunity and are used for tumor modeling and for evaluating drug effects [35–37].

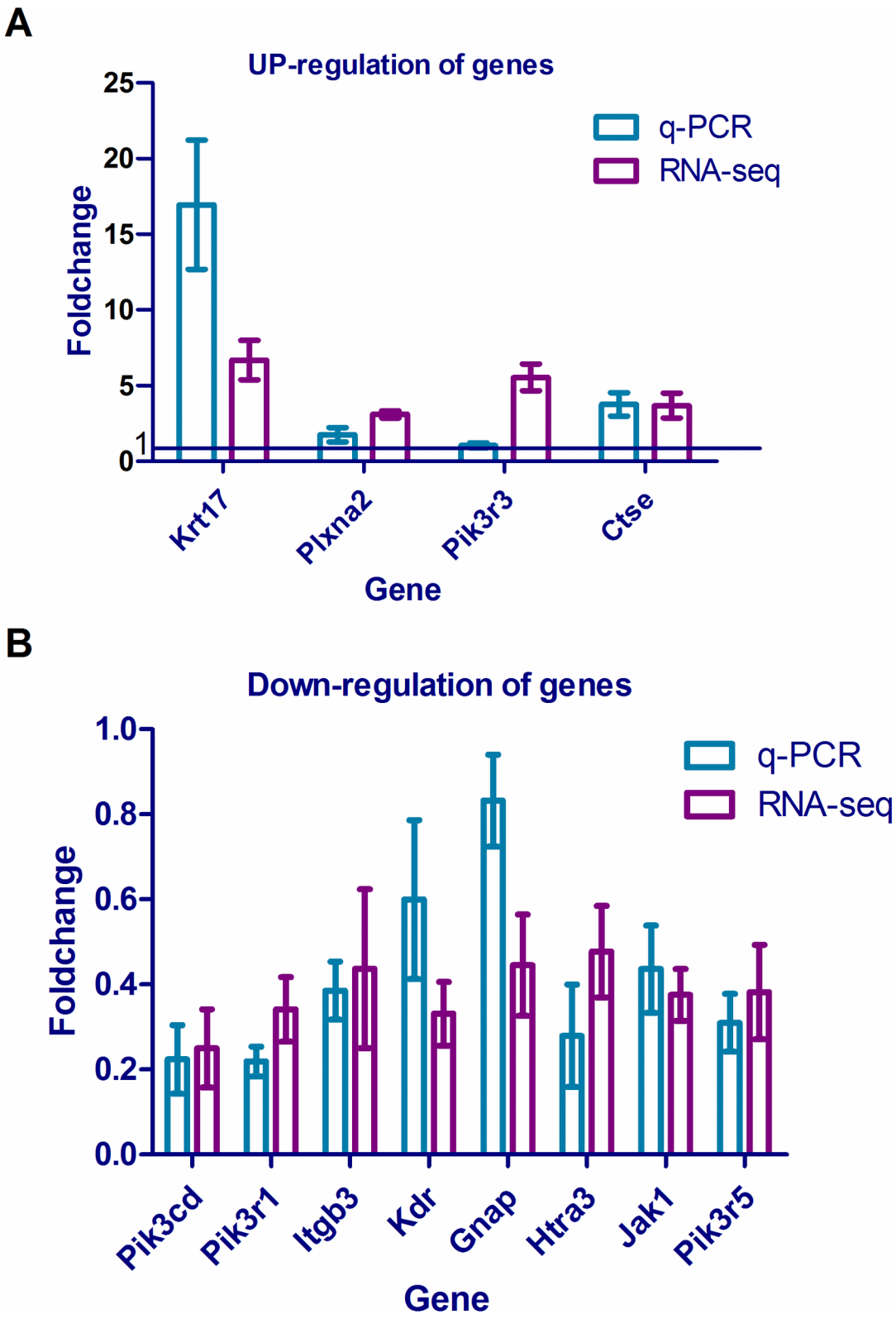


**Fig 8. Confirmation of RNA-Seq results by q-PCR.** A: Four up-regulated genes (*Krt17*, *Plxna2*, *Pik3r3* and *Ctse*). B: Eight down-regulated genes (*Pik3r1*, *Pik3cd*, *Itgb3*, *Kdr*, *Gnaq*, *Htra3*, *Jak1* and *Pik3r5*).

https://doi.org/10.1371/journal.pone.0182463.g008

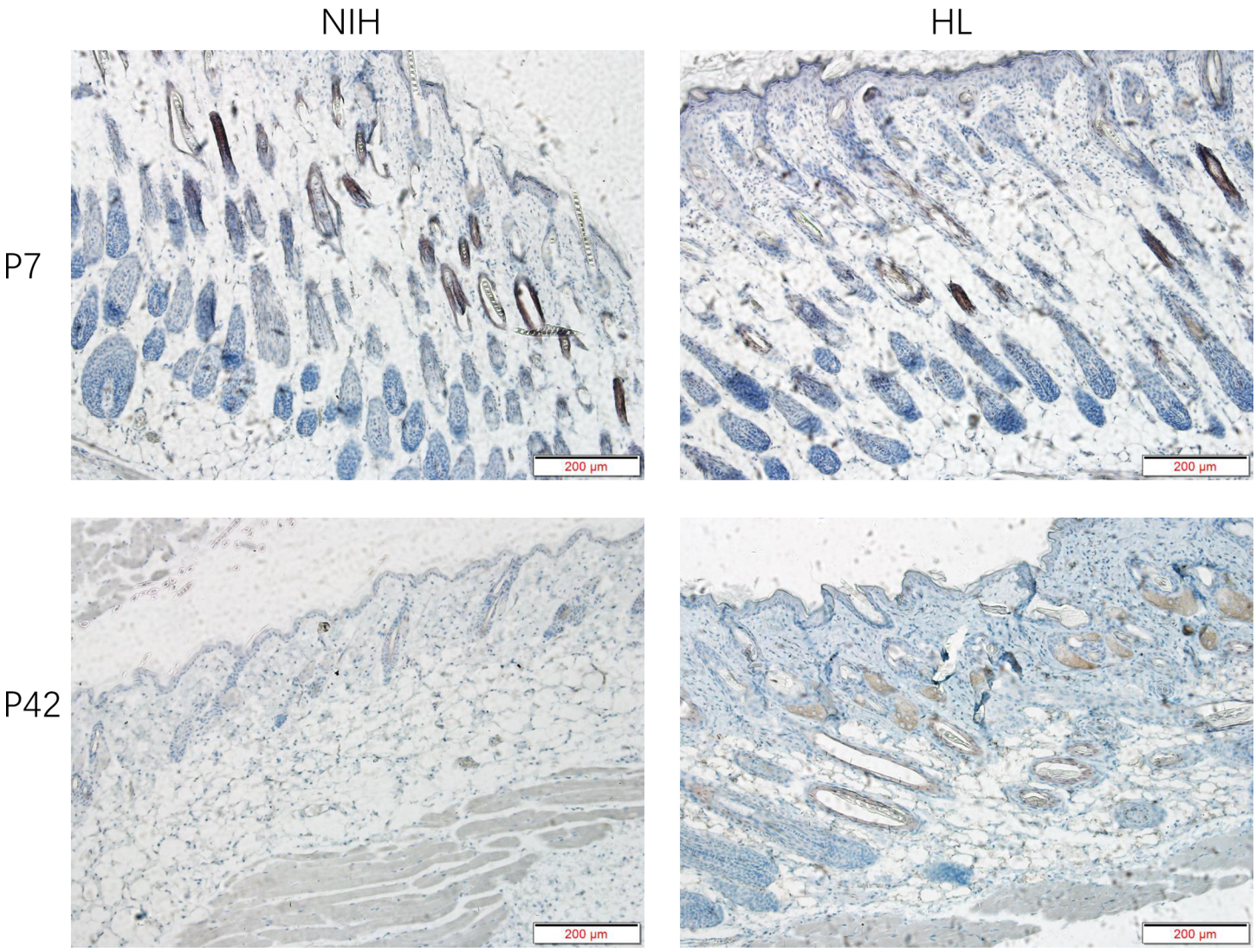


**Fig 9. Expression of Pik3r1 protein in tissue sections.** The Pik3r1 antibody shows signals in partial hair follicles. In addition, the sebaceous glands also show some Pik3r1 expression.

https://doi.org/10.1371/journal.pone.0182463.g009

Another model is the hairpoor mouse ($hr^{hp}$), which was generated via N-ethyl-N-nitrosourea (ENU) mutagenesis and has a coat of abnormal hairs [55]; this mouse was found to have a point mutation in the hairless gene, making it a good animal model for studying the human familial genetic disease Marie Unna hereditary hypotrichosis (MUHH). We found that NIH hairless mice exhibit hair follicle developmental disorders in the first hair growth cycle. Additionally, other researchers have reported progressive hair loss and abnormal hair growth cycles in these mice.

We used RNA-Seq high-throughput sequencing technology [38–40] to examine and compare the phenotypes and skin structures of six-week-old female NIH normal and NIH HL mice. We found that keratinization, epidermis development, hair follicle development and skin development were up-regulated in NIH hairless mice. H&E staining of P42 skin slices showed that in NIH normal mice, the second hair growth cycle was in telogen, whereas in HL mice, the hair growth cycle was still in anagen. The innate immune response, immune

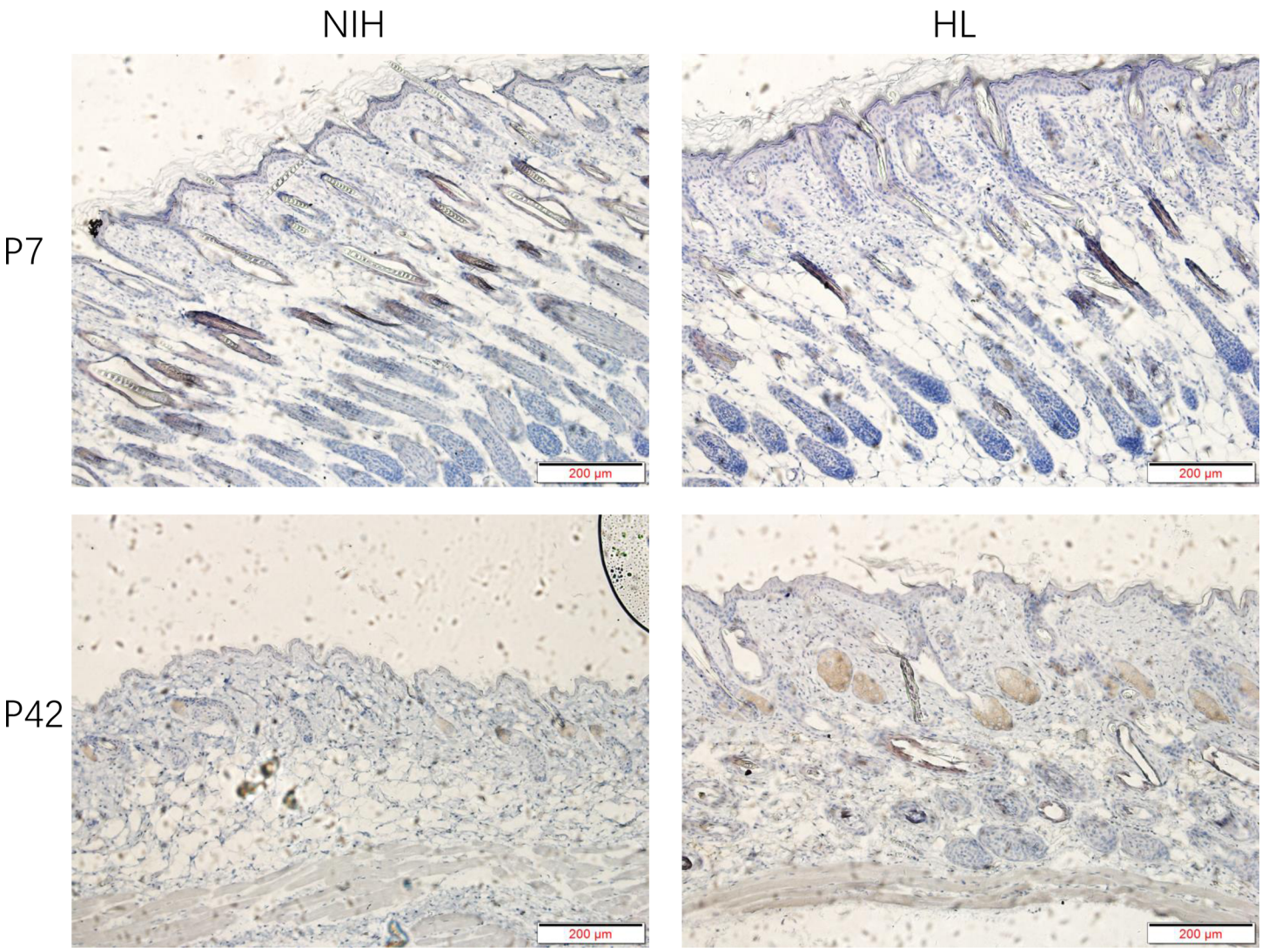


**Fig 10. Expression of Pik3r3 protein in tissue sections.** The Pik3r3 antibody shows an expression pattern similar to that of the Pik3r1 antibody.

https://doi.org/10.1371/journal.pone.0182463.g010

response, viral response and other pathways closely associated with immune defense showed downward trends, indicating abnormal immune function in NIH hairless mice [41–43]. These results are consistent with the spontaneous tumor formation that occurs when breeding NIH hairless mice. Pathway analysis showed that genes involved in basal cell carcinoma, the cell cycle and the Hippo, Hedgehog and Wnt signaling pathways were up-regulated in HL mice; these pathways are associated with cell proliferation, growth, cycle, organ size and cancer [30, 44]. In contrast, genes involved in signal transduction, receptor-mediated signaling (e.g., calcium, cytokine-cytokine receptor, and PI3K-Akt signaling) and bacterial and parasitic infection (e.g., *Staphylococcus aureus* infection) were down-regulated in HL mice.

Because many genes might affect the screening of core genes and the construction of the interaction network, we used WGCNA to classify genes based on their expression patterns and to categorize the modules by color (the turquoise modules are closely related to our research aims). To further understand the importance of gene and pathway interactions and to screen for key genes and pathways that play significant roles in the case group (NIH hairless mice),

we built two gene interaction networks and one pathway interaction network based on the direct or systemic interactions assigned between pathways in the KEGG database. Based on the degrees of involvement of the genes in the network, *Pik3r1*, *Pik3r3*, *Pik3cd*, *Kdr*, *Itgb3* and *Itgb7* were identified as key genes.

Previous studies have shown that the PI3K / AKT signaling pathway is involved in cell regulation processes, including cell growth, proliferation, transformation, epithelial-to-mesenchymal transition and survival, and cell pathology [45–47]. Disruption of the PI3K / AKT signaling pathway can lead to cell growth, proliferation and survival disorders, thus affecting normal bodily activities. Studies of the *Pik3r1* gene have described its association with the occurrence and metastasis of cancer [48–50]. Notably, the analysis of atopic dermatitis sequencing data revealed a crucial role for *Pik3r1* in atopic dermatitis [30, 51]. However, research on its involvement in hair follicle development is lacking. Finally, we found that *Pik3r1* and *Pik3r3* proteins were specifically expressed by hair follicles.

In summary, we constructed gene expression profiles for the skin of six-week-old NIH hairless and NIH normal mice. A bioinformatics analysis of the 5,068 DEGs revealed differences in the cell cycle, immune response and skin development. Screening of the *Pik3r1* and *Pik3r3* genes will be of great importance in our future research.

## Supporting information

**S1 Table. Quality control.**
(XLSX)

**S2 Table. Mapping statistics.**
(XLSX)

**S1 File. Differential gene expression analysis (FC $\geq$ 2, FDR $<$ 0.05).**
(XLSX)

**S2 File. GO analysis of the differentially expressed genes (BP).**
(XLSX)

**S3 File. GO analysis of the differentially expressed genes (CC).**
(XLSX)

**S4 File. GO analysis of the differentially expressed genes (MF).**
(XLSX)

**S5 File. Pathway analysis of the differentially expressed genes.**
(XLSX)

**S6 File. Weighted gene co-expression network analysis.**
(XLS)

**S7 File. q-PCR verification.**
(DOCX)

**S8 File. Raw data for Fig 7.**
(XLSX)

## Author Contributions

**Conceptualization:** Bao Yuan, Wen-Zhi Ren.

**Data curation:** Zhong-Hao Ji, Jian Chen.

**Formal analysis:** Zhong-Hao Ji, Jian Chen.

**Funding acquisition:** Bao Yuan, Wen-Zhi Ren.

**Investigation:** Zhong-Hao Ji, Jian Chen, Wei Gao, Jin-Yu Zhang, Fu-Shi Quan, Jin-Ping Hu.

**Resources:** Wei Gao, Jin-Yu Zhang, Fu-Shi Quan, Jin-Ping Hu.

**Supervision:** Bao Yuan, Wen-Zhi Ren.

**Visualization:** Zhong-Hao Ji, Jian Chen.

**Writing – original draft:** Zhong-Hao Ji, Jian Chen.

**Writing – review & editing:** Bao Yuan, Wen-Zhi Ren.

## References


1. Bichsel KJ, Gogia N, Malouff T, Pena Z, Forney E, Hammiller B, et al. Role for the epidermal growth factor receptor in chemotherapy-induced alopecia. PloS one. 2013; 8(7):e69368. https://doi.org/10.1371/journal.pone.0069368 PMID: 23894460; PubMed Central PMCID: PMC3716704.
2. Wang L, Xu W, Cao L, Tian T, Yang M, Li Z, et al. Differential Expression of Proteins Associated with the Hair Follicle Cycle—Proteomics and Bioinformatics Analyses. PloS one. 2016; 11(1):e0146791. https://doi.org/10.1371/journal.pone.0146791 PMID: 26752403; PubMed Central PMCID: PMC4709225.
3. Nam Y, Kim JK, Cha DS, Cho JW, Cho KH, Yoon S, et al. A novel missense mutation in the mouse hairless gene causes irreversible hair loss: genetic and molecular analyses of Hr m1Enu. Genomics. 2006; 87(4):520–6. https://doi.org/10.1016/j.ygeno.2005.12.005 PMID: 16455232.
4. Araujo VC, Fukutani KF, Oshiro ET, Rodrigues PO, Rizk YS, Carollo CA, et al. Hairless mice as an experimental model of infection with Leishmania (Leishmania) amazonensis. Experimental parasitology. 2015; 157:138–44. https://doi.org/10.1016/j.exppara.2015.07.010 PMID: 26234915.
5. Baek IC, Kim JK, Cho KH, Cha DS, Cho JW, Park JK, et al. A novel mutation in Hr causes abnormal hair follicle morphogenesis in hairpoor mouse, an animal model for Marie Unna Hereditary Hypotrichosis. Mammalian genome: official journal of the International Mammalian Genome Society. 2009; 20 (6):350–8. https://doi.org/10.1007/s00335-009-9191-8 PMID: 19513791.
6. Kim BK, Lee HY, Kim I, Choi K, Park J, Yoon SK. Increased expression of Dkk1 by HR is associated with alteration of hair cycle in hairpoor mice. Journal of dermatological science. 2014; 74(1):81–7. https://doi.org/10.1016/j.jdermsci.2013.12.007 PMID: 24447645.
7. Kwack MH, Kim MK, Kim JC, Sung YK. Dickkopf 1 promotes regression of hair follicles. The Journal of investigative dermatology. 2012; 132(6):1554–60. https://doi.org/10.1038/jid.2012.24 PMID: 22358062.
8. Kim SN, Jo GH, Kim HA, Heo Y. Aberrant IgG isotype generation in mice with abnormal behaviors. Journal of immunotoxicology. 2016; 13(1):92–6. https://doi.org/10.3109/1547691X.2015.1014581 PMID: 25691089.
9. Liu Y, Das S, Olszewski RE, Carpenter DA, Culiat CT, Sundberg JP, et al. The near-naked hairless (Hr (N)) mutation disrupts hair formation but is not due to a mutation in the Hairless coding region. The Journal of investigative dermatology. 2007; 127(7):1605–14. https://doi.org/10.1038/sj.jid.5700755 PMID: 17330134.
10. Nakamura M, Schneider MR, Schmidt-Ullrich R, Paus R. Mutant laboratory mice with abnormalities in hair follicle morphogenesis, cycling, and/or structure: an update. Journal of dermatological science. 2013; 69(1):6–29. https://doi.org/10.1016/j.jdermsci.2012.10.001 PMID: 23165165.
11. Chen J, Yuan B, Zhu T, Cai Y, Hu J-P, Gao Y, et al. Reproductive performance and histological characteristics of select organs in NIH hairless mice. International journal of clinical and experimental medicine. 2016; 9(6):8925–33.
12. Kim BK, Baek IC, Lee HY, Kim JK, Song HH, Yoon SK. Gene expression profile of the skin in the 'hairpoor' (HrHp) mice by microarray analysis. BMC genomics. 2010; 11:640. https://doi.org/10.1186/1471-2164-11-640 PMID: 21083932; PubMed Central PMCID: PMC3091768.
13. Cai Z, Jiang X, Pan Y, Chen L, Zhang L, Zhu K, et al. Transcriptomic analysis of hepatic responses to testosterone deficiency in miniature pigs fed a high-cholesterol diet. BMC genomics. 2015; 16:59. https://doi.org/10.1186/s12864-015-1283-0 PMID: 25887406; PubMed Central PMCID: PMC4328429.
14. Li XF, Cao RB, Luo J, Fan JM, Wang JM, Zhang YP, et al. MicroRNA transcriptome profiling of mice brains infected with Japanese encephalitis virus by RNA sequencing. Infection, genetics and evolution:

journal of molecular epidemiology and evolutionary genetics in infectious diseases. 2016; 39:249–57. https://doi.org/10.1016/j.meegid.2016.01.028 PMID: 26845346.

15. Miao X, Qin QL. Genome-wide transcriptome analysis of mRNAs and microRNAs in Dorset and Small Tail Han sheep to explore the regulation of fecundity. Molecular and cellular endocrinology. 2015; 402:32–42. https://doi.org/10.1016/j.mce.2014.12.023 PMID: 25573241.

16. Ouyang Y, Pan J, Tai Q, Ju J, Wang H. Transcriptomic changes associated with DKK4 overexpression in pancreatic cancer cells detected by RNA-Seq. Tumour biology: the journal of the International Society for Oncodevelopmental Biology and Medicine. 2016; 37(8):10827–38. https://doi.org/10.1007/s13277-015-4379-x PMID: 26880586.

17. Ashburner M, Ball CA, Blake JA, Botstein D, Butler H, Cherry JM, et al. Gene ontology: tool for the unification of biology. The Gene Ontology Consortium. Nat Genet. 2000; 25(1):25–9. https://doi.org/10.1038/75556 PMID: 10802651; PubMed Central PMCID: PMC3037419.

18. Dupuy D, Bertin N, Hidalgo CA, Venkatesan K, Tu D, Lee D, et al. Genome-scale analysis of in vivo spatiotemporal promoter activity in Caenorhabditis elegans. Nat Biotechnol. 2007; 25(6):663–8. https://doi.org/10.1038/nbt1305 PMID: 17486083.

19. Schlitt T, Palin K, Rung J, Dietmann S, Lappe M, Ukkonen E, et al. From gene networks to gene function. Genome research. 2003; 13(12):2568–76. https://doi.org/10.1101/gr.1111403 PMID: 14656964; PubMed Central PMCID: PMC403798.

20. Klipper-Aurbach Y, Wasserman M, Braunspiegel-Weintrob N, Borstein D, Peleg S, Assa S, et al. Mathematical formulae for the prediction of the residual beta cell function during the first two years of disease in children and adolescents with insulin-dependent diabetes mellitus. Med Hypotheses. 1995; 45 (5):486–90. PMID: 8748093.

21. Jansen R, Lan N, Qian J, Gerstein M. Integration of genomic datasets to predict protein complexes in yeast. J Struct Funct Genomics. 2002; 2(2):71–81. PMID: 12836664.

22. Tecson Mendoza EM, CL A, Botella JR. Recent advances in the development of transgenic papaya technology. Biotechnol Annu Rev. 2008; 14:423–62. https://doi.org/10.1016/S1387-2656(08)00019-7 PMID: 18606373.

23. Wei Z, Li M. Genome-wide linkage and association analysis of rheumatoid arthritis in a Canadian population. BMC Proc. 2007; 1 Suppl 1:S19. PMID: 18466515; PubMed Central PMCID: PMC2359870.

24. Spirin VF, Varshamov LA. [Work conditions and occupational morbidity among agricultural workers]. Med Tr Prom Ekol. 2003;(11):1–4. PMID: 14752897.

25. Langfelder P, Horvath S. WGCNA: an R package for weighted correlation network analysis. BMC bioinformatics. 2008; 9:559. https://doi.org/10.1186/1471-2105-9-559 PMID: 19114008; PubMed Central PMCID: PMC2631488.

26. Barabasi AL, Oltvai ZN. Network biology: understanding the cell's functional organization. Nat Rev Genet. 2004; 5(2):101–13. https://doi.org/10.1038/nrg1272 PMID: 14735121.

27. Ravasz E, Somera AL, Mongru DA, Oltvai ZN, Barabasi AL. Hierarchical organization of modularity in metabolic networks. Science. 2002; 297(5586):1551–5. https://doi.org/10.1126/science.1073374 PMID: 12202830.

28. Carlson MR, Zhang B, Fang Z, Mischel PS, Horvath S, Nelson SF. Gene connectivity, function, and sequence conservation: predictions from modular yeast co-expression networks. BMC genomics. 2006; 7:40. https://doi.org/10.1186/1471-2164-7-40 PMID: 16515682; PubMed Central PMCID: PMC1413526.

29. Pazhamala LT, Agarwal G, Bajaj P, Kumar V, Kulshreshtha A, Saxena RK, et al. Deciphering Transcriptional Programming during Pod and Seed Development Using RNA-Seq in Pigeonpea (Cajanus cajan). PLoS One. 2016; 11(10):e0164959. https://doi.org/10.1371/journal.pone.0164959 PMID: 27760186; PubMed Central PMCID: PMC5070767.

30. Herbert Pratt C, Potter CS, Fairfield H, Reinholdt LG, Bergstrom DE, Harris BS, et al. Dsp rul: a spontaneous mouse mutation in desmoplakin as a model of Carvajal-Huerta syndrome. Experimental and molecular pathology. 2015; 98(2):164–72. https://doi.org/10.1016/j.yexmp.2015.01.015 PMID: 25659760; PubMed Central PMCID: PMC4388778.

31. Slominski AT, Zmijewski MA, Skobowiat C, Zbytek B, Slominski RM, Steketee JD. Sensing the environment: regulation of local and global homeostasis by the skin's neuroendocrine system. Adv Anat Embryol Cell Biol. 2012; 212:v, vii, 1–115. PMID: 22894052; PubMed Central PMCID: PMC3422784.

32. Morifuji M, Oba C, Ichikawa S, Ito K, Kawahata K, Asami Y, et al. A novel mechanism for improvement of dry skin by dietary milk phospholipids: Effect on epidermal covalently bound ceramides and skin inflammation in hairless mice. Journal of dermatological science. 2015; 78(3):224–31. https://doi.org/10.1016/j.jdermsci.2015.02.017 PMID: 25816721.

33. Slominski AT, Manna PR, Tuckey RC. On the role of skin in the regulation of local and systemic steroidogenic activities. Steroids. 2015; 103:72–88. https://doi.org/10.1016/j.steroids.2015.04.006 PMID: 25988614; PubMed Central PMCID: PMC4631694.

34. Slominski AT, Zmijewski MA, Zbytek B, Tobin DJ, Theoharides TC, Rivier J. Key role of CRF in the skin stress response system. Endocr Rev. 2013; 34(6):827–84. https://doi.org/10.1210/er.2012-1092 PMID: 23939821; PubMed Central PMCID: PMC3857130.

35. Fang W, Fan Y, Fa Z, Xu J, Yu H, Li P, et al. microRNA-625 inhibits tumorigenicity by suppressing proliferation, migration and invasion in malignant melanoma. Oncotarget. 2017. https://doi.org/10.18632/oncotarget.14710 PMID: 28129648.

36. He S, Cen B, Liao L, Wang Z, Qin Y, Wu Z, et al. A tumor-targeting cRGD-EGFR siRNA conjugate and its anti-tumor effect on glioblastoma in vitro and in vivo. Drug delivery. 2017; 24(1):471–81. https://doi.org/10.1080/10717544.2016.1267821 PMID: 28181832.

37. Yin H, Huang X, Tao M, Hu Q, Qiu J, Chen W, et al. Adenovirus-mediated TIPE2 overexpression inhibits gastric cancer metastasis via reversal of epithelial-mesenchymal transition. Cancer gene therapy. 2017. https://doi.org/10.1038/cgt.2017.3 PMID: 28186089.

38. Leshkowitz D, Feldmesser E, Friedlander G, Jona G, Ainbinder E, Parmet Y, et al. Using Synthetic Mouse Spike-In Transcripts to Evaluate RNA-Seq Analysis Tools. PloS one. 2016; 11(4):e0153782. https://doi.org/10.1371/journal.pone.0153782 PMID: 27100792; PubMed Central PMCID: PMC4839710.

39. Ma Q, Wu M, Pei W, Wang X, Zhai H, Wang W, et al. RNA-Seq-Mediated Transcriptome Analysis of a Fiberless Mutant Cotton and Its Possible Origin Based on SNP Markers. PloS one. 2016; 11(3): e0151994. https://doi.org/10.1371/journal.pone.0151994 PMID: 26990639; PubMed Central PMCID: PMC4798417.

40. Tsai CC, Shih HC, Wang HV, Lin YS, Chang CH, Chiang YC, et al. RNA-Seq SSRs of Moth Orchid and Screening for Molecular Markers across Genus Phalaenopsis (Orchidaceae). PloS one. 2015; 10(11): e0141761. https://doi.org/10.1371/journal.pone.0141761 PMID: 26523377; PubMed Central PMCID: PMC4629892.

41. Troy NM, Bosco A. Respiratory viral infections and host responses; insights from genomics. Respiratory research. 2016; 17(1):156. https://doi.org/10.1186/s12931-016-0474-9 PMID: 27871304; PubMed Central PMCID: PMC5117516.

42. Hatesuer B, Hoang HT, Riese P, Trittel S, Gerhauser I, Elbahesh H, et al. Deletion of Irf3 and Irf7 Genes in Mice Results in Altered Interferon Pathway Activation and Granulocyte-Dominated Inflammatory Responses to Influenza A Infection. Journal of innate immunity. 2016. https://doi.org/10.1159/000450705 PMID: 27811478.

43. Drokhlyansky E, Goz Ayturk D, Soh TK, Chrenek R, O'Loughlin E, Madore C, et al. The brain parenchyma has a type I interferon response that can limit virus spread. Proceedings of the National Academy of Sciences of the United States of America. 2017; 114(1):E95–E104. https://doi.org/10.1073/pnas.1618157114 PMID: 27980033; PubMed Central PMCID: PMC5224383.

44. Iglesias-Bartolome R, Torres D, Marone R, Feng X, Martin D, Simaan M, et al. Inactivation of a Galpha (s)-PKA tumour suppressor pathway in skin stem cells initiates basal-cell carcinogenesis. Nature cell biology. 2015; 17(6):793–803. https://doi.org/10.1038/ncb3164 PMID: 25961504; PubMed Central PMCID: PMC4449815.

45. Jiang J, Wang B, Li J, Ye B, Lin S, Qian W, et al. Total coumarins of Hedyotis diffusa induces apoptosis of myelodysplastic syndrome SKM-1 cells by activation of caspases and inhibition of PI3K/Akt pathway proteins. Journal of ethnopharmacology. 2017; 196:253–60. https://doi.org/10.1016/j.jep.2016.12.012 PMID: 27988397.

46. Shao L, Li H, Chen J, Song H, Zhang Y, Wu F, et al. Irisin suppresses the migration, proliferation, and invasion of lung cancer cells via inhibition of epithelial-to-mesenchymal transition. Biochemical and biophysical research communications. 2016. https://doi.org/10.1016/j.bbrc.2016.12.084 PMID: 27986567.

47. Yang K, Zhang H, Luo Y, Zhang J, Wang M, Liao P, et al. Gypenoside XVII Prevents Atherosclerosis by Attenuating Endothelial Apoptosis and Oxidative Stress: Insight into the ERalpha-Mediated PI3K/Akt Pathway. International journal of molecular sciences. 2017; 18(2). https://doi.org/10.3390/ijms18020077 PMID: 28208754.

48. Kobayashi H, Chang SH, Mori D, Itoh S, Hirata M, Hosaka Y, et al. Biphasic regulation of chondrocytes by Rela through induction of anti-apoptotic and catabolic target genes. Nature communications. 2016; 7:13336. https://doi.org/10.1038/ncomms13336 PMID: 27830706; PubMed Central PMCID: PMC5109547.

49. Packer L, Geng X, Bonazzi VF, Ju R, Mahon C, Cummings MC, et al. PI3K inhibitors synergize with FGFR inhibitors to enhance antitumor responses in FGFR2-mutant endometrial cancers. Molecular cancer therapeutics. 2017. https://doi.org/10.1158/1535-7163.MCT-16-0415 PMID: 28119489.

**50.** Peng X, Xue H, Lu L, Shi P, Wang J, Wang J. Accumulated promoter methylation as a potential biomarker for esophageal cancer. Oncotarget. 2017; 8(1):679–91. https://doi.org/10.18632/oncotarget.13510 PMID: 27893424.

**51.** Zhang ZK, Yang Y, Bai SR, Zhang GZ, Liu TH, Zhou Z, et al. Screening for key genes associated with atopic dermatitis with DNA microarrays. Molecular medicine reports. 2014; 9(3):1049–55. https://doi.org/10.3892/mmr.2014.1908 PMID: 24452877.